Nanofluidic tools for bioanalysis : the large advantages of the nano-scale

Janssen, K.G.H.

CHAPTER 2

Solution Titration by Wall Deprotonation During Capillary Filling of Silicon Oxide Nanochannels[a]

2.1 Abstract

This paper describes a fundamental challenge when using silicon oxide nanochannels for analytical systems, namely the occurrence of a strong proton release or proton uptake from the walls in any transient situation such as channel filling. Experimentally, when fluorescein solutions were introduced into silicon oxide nanochannels through capillary pressure, a distinct bisection of the fluorescence was observed, the zone of the fluid near the entrance fluoresced, while the zone near the meniscus, was dark. The ratio between the zones was found to be constant in time and to depend on ionic strength, pH and the presence of a buffer and its characteristics. Theoretically, using the Gouy-Chapman-Stern model of the electrochemical double-layer, we demonstrate that this phenomenon can be effectively modeled as a titration of the solution by protons released from silanol groups on the walls, as a function of the pH and ionic strength of the introduced solution. The results demonstrate the dominant influence of the surface on the fluid composition in nanofluidic experiments, in transient situations such as filling, and changes in solvent properties such as the pH or ionic strength. The implications of these fundamental properties of silicon oxide nanochannels are important for analytical strategies and in particular the analysis of complex biological samples.

[a]Published as: Kjeld G. H. Janssen, Hanh T. Hoang, Jan Floris, Jeroen de Vries, Niels R. Tas, and Jan C. T. Eijkel and Thomas Hankemeier, *Analytical Chemistry*, **80**, 8095-8101 (2008).

2.2 Introduction

The fabrication and application of nanochannels have gained considerable interest in the past few years. Using bonding, 1D nanochannels are mostly formed by shallow etching of trenches in silicon (or glass) wafers followed by bonding to glass (or silicon) cover wafers to form enclosed channels[43,78]. 2D nanochannels can be fabricated using nanolithography[79–81], surface- and bulk- machining[82,83] and electrospinning[84]. Nanochannels are created in various types of materials such as silicon (silicon oxide, silicon nitride), glass and polymers[85,86]. An extensive review on fabrication was made by Mijatovic et al.[87].

Channels with such small dimensions are of interest because due to the extremely high surface to volume ratio, (electrical) interface effects between the fluid and channel wall surfaces become dominant[42]. For example, S. Pennathur et al.[88,89] described a novel nanoscale electrophoretic separation method in a theoretical and experimental study on the electrokinetic transport in nanochannels. Pu et al.[49] demonstrated an ion-enrichment and ion-depletion effect when an electric field was applied across two reservoirs connected by 60 nm deep channels.

Less known, the surface chemistry of silicon oxide has a large influence on solutions in nanochannels. It has been known for a very long time that the silanol groups present on silica are capable of protonating the solution in contact with it. Actually, this effect has been used to assess the presence of silanol groups on silica beads in chromatographic columns via the indicator methyl red which colors red at a pH below 4.4[90].

2.2.1 General description of the phenomenon and hypothesis.

In this paper we demonstrate that a solution introduced into an empty silicon oxide nanochannel is acidified and dissolved substances protonated. For this purpose we measured the fluorescence of solutions of fluorescein, which has a strong pH-dependent fluorescence, introduced in empty channels through capillary pressure. During filling, two distinct zones were observed, with the zone of the solution starting from the entrance showing fluorescence, while in the zone near the flow front no fluorescence was observed, as shown in Figure 2.1. The movie belonging to this experiment, showing the filling of the nanochannel and the progression in time of the two zones, has been provided in the electronic supporting information at the ACS publications website belonging to the paper this chapter is adapted from, Movie S-1.

To study this phenomenon in more detail we varied pH, buffer concentration and ionic strength and determined for various solution compositions the ratio of the lengths of the fluorescing and dark zones. From this ratio we calculated the number of protons released per m^2 and compared these data with a model based on oxide surface chemistry theory[91] which predicts the amount of released pro-

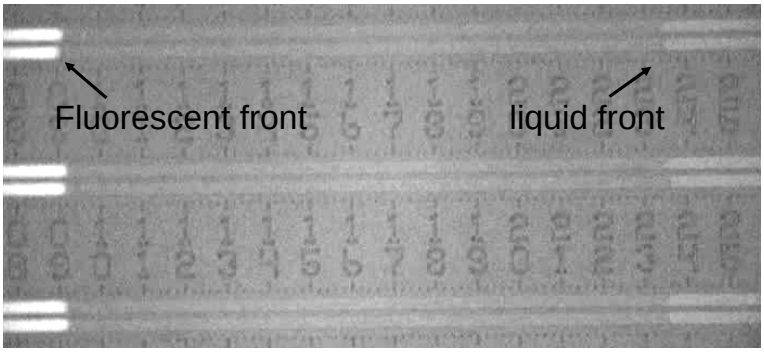

Figure 2.1 Typical image of fluorescence observed in nanochannels during filling. In this experiment, (experiment. no. 1 of Table 2.1, screenshot of Movie S-1), the partial filling of parallel channels, 20 µm wide and 40.5 nm deep, taken at t = 5 s, are shown. From left to right the channel is filling from the reservoir, which is outside the image shown. Fluorescence is observed in the filled zone, from x = 0 to x = 0.92 mm, but not in the zone from x = 0.92 mm to 2.36 mm.

tons. The results obtained describe an effect relevant for nanofluidic experiments because they indicate the influence of the surface chemistry on fluid composition such as pH and wall charge in transient situations.

2.2.2 Considerations of relevance of other nanochannel effects.

Ion exclusion of the negatively charged fluorescein was first considered as a possible explanation of the observed phenomenon, but discarded since the phenomenon became more pronounced with increasing ionic strength. For the same reason also the generation of a streaming potential was discarded as an explanation. Straightforward retention due to adsorption to the wall, as in thin layer chromatography, which could become significant due to the high surface to volume ratio, can also be ruled out. S. Pennathur et al.[89] in fact demonstrated experimentally that fluorescein effectively travels faster instead of slower through silicon oxide nanochannels as compared to microchannels, due to exclusion of the negative ion from the double layer. A final argument to support the titration theory is that experiments we performed with a pH-insensitive dye (Alexa, molecular probes; data not shown) showed no significant lagging of the fluorescent front.

2.2.3 Chip manufacture.

Chip devices containing micro- and nanochannels were fabricated based on the approach of Haneveld et al[43]. Nanochannels and microchannels (including rulers for filling observation) were manufactured in the bottom-side silicon wafers by wet

chemical etching and reactive ion etching, respectively. After etching, a dry thermal oxide of 20 nm thickness was grown on the silicon wafers to ensure adequate surface hydrophilicity for capillary filling of the nanochannels. The etch depths of the channel structures were measured with a mechanical surface profiler (Dektak 8, Veeco Instruments Inc., Plainview, NY, USA). The processing of the top-side Borofloat glass wafers consisted of powder blasting of access holes followed by thorough wafer cleaning to remove residue from the abrasive powder blasting particles. Prior to prebonding the top and bottom wafers were Piranha cleaned. This step was followed by fusion bonding at 400°C for 4 hours, to ensure identical starting conditions for the experiments. For a layout of the channel structure, see Figure 2.2. Directly prior to the experiments the wafers were conditioned by heating for 2 hours at 400°C, to ensure identical starting conditions for the experiments.

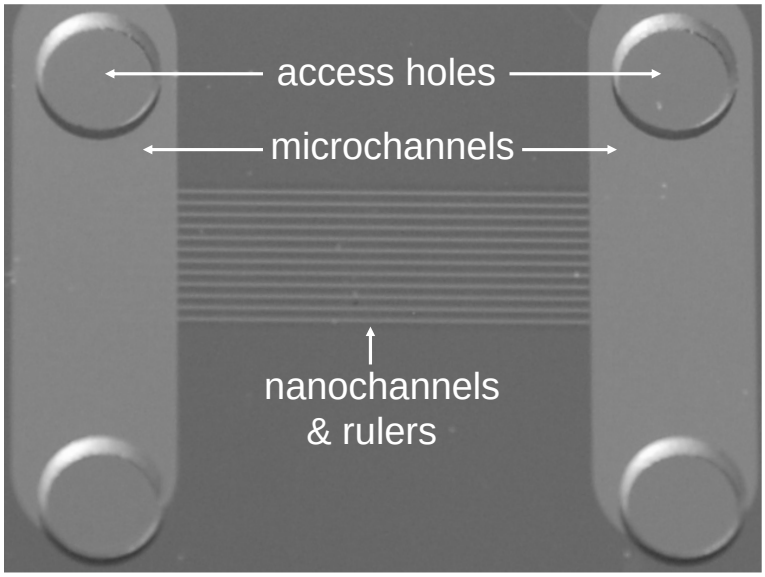

Figure 2.2 Chip layout seen from the top. Vertically, the microchannels connecting the two pairs of access holes can be seen and between them the rulers positioned along the nanochannels are visible. The nanochannels are 50 nm deep and 20 µm wide, the microchannels are 20 µm deep, 15 mm long and 4 mm wide.

2.2.4 Fluorescence measurements.

To probe the pH in the nanochannels, we used the fluorescent activity of disodiumfluoresceine (Sigma-Aldrich, St. Louis, MO, USA). Depending on the pH, fluorescein can have a double or single negative charge or be neutral; the single negatively charged form has a pK_a of 6.68 and the neutral form has an apparent

pK_a of 4.34[92]. When the molecule is excited at 488 nm and emission is measured at 514 nm, the molar response of the ion having a valence of -1 is only 5.7% and that of the neutral form 0.8%[93] in comparison to the ion having valence -2; therefore the emission can be used as an indicator of the local pH.

Measurements were done on a fluorescence microscope (Leica DM LM, Wetzlar, Germany), using a 100 W mercury lamp, an I3 filter cube and a 510 nm dichromatic mirror. Movies were taken with a CCD camera to record the movement of the solutions entering the empty nanochannels and analyzed using Pinnacle software (Pinnacle, Mountain View, CA, USA). From the parallel channels one was selected for measurement, as differences between parallel channels were small (see Fig 2.1).

2.2.5 Composition of the introduced solutions.

To buffer the solutions, 2-amino-2-(hydroxymethyl)propane-1,3-diol (TRIS) was used, having a pK_a of 8.06 (Merck & Co., Inc., Whitehouse Station, NJ, USA). To influence the ionic strength, various amounts of potassium chloride (KCl) (Sigma-Aldrich, St. Louis, MO, USA) were added. The composition of the solutions introduced in the channels were all made in deionized water (0.7 µS/cm) and are described in Table 2.1.

Table 2.1 Composition of the solution, the height (h) of the channel and the measured pH for the various experiments.

Expt	(mol/L) of			h(nm)	pH
	Tris	HCl	KCl		
1	0	0	0	40.5	7.3
2	0	0	0	49.0	7.4
3	0	0	0.1	48.0	7.1
4	0	0	0.1	49.0	7.2
5	0	0	0.2	52.8	7.2
6	0	0	0.2	44.0	7.1
7	0	0	0.5	47.8	7.1
8	0	0	0.5	47.0	7.0
9	0.2	0.073	0	50.0	8.6
10	0.2	0.073	0	50.3	8.4
11	0.2	0.073	0.1	49.8	8.4
12	0.2	0.073	0.2	50.3	8.4
13	0.2	0.073	0.5	45.5	8.5
14	0.2	0.073	0.5	48.4	8.4
15	1	0.364	0	49.5	8.5

2.3 Theory

2.3.1 Capillary filling.

The walls of the nanochannels in the chip device are assumed to have hydrophilic silanol groups. When liquid comes into contact with such a nanochannel, the liquid is pulled into the empty channel by capillary forces creating a pressure gradient ΔP (Pa),

$$\Delta P = \frac{-2\gamma\cos\theta}{h} \tag{2.1}$$

with γ the gas liquid surface tension (Nm^{-1}), θ the contact angle and h the channel height. The position, x(m), of the liquid front in a nanochannel at any point in time, t(s), is given in accordance with the Washburn equation for a rectangular channel with the condition: width $>>$ height[94,95], and viscosity μ (Pa·s):

$$x = \sqrt{\frac{\gamma h t\cos\theta}{3\mu}} \tag{2.2}$$

2.3.2 Experimental amount of protons released.

We explain the phenomenon observed in Figure 2.3, as follows. As the aqueous solution is introduced into the nanochannel from the reservoir, protons are released from the wall into the solution, lowering the pH as well as protonating compounds in the solution. When the fluid flows along the channel, the front of the fluid continuously comes into contact with a new section of the wall, with which it anew establishes equilibrium, again taking up protons. This process continues until the fluid in the liquid front reaches a pH corresponding to the point of zero charge (pzc) of SiO_2, which is on the order of $pH_{pzc} = 2-3$. At a pH of the fluid below this pH_{pzc} the wall will no longer release protons. On the other hand, the zone of fluid behind the front comes into contact with a wall already in equilibrium with a solution of this composition. As a result, the fluorescein is no longer protonated, and the zone near the entrance will maintain its fluorescent activity (see Figure 2.3).

We assume infinitely fast (de)protonation reactions ($\propto$ fs) and we calculated the diffusion time, from the wall to the center of the channel, using Einstein-Smoluchowski[96], to be 35 ns. Therefore for our experiments we assume the onset of radial equilibrium due to the small dimension of the channel to be infinitely fast. The time scale of the axial diffusion of protons ($\propto 1000$ s for an average diffusion distance of half the channel length) is 1 order of magnitude larger than the timescale of filling the channel ($\propto 100$s). For our calculations we will assume that the pH change from that of the introduced solution to the pH_{pzc} occurs abruptly at the fluorescent front. In the Results and Discussion we will show the validity of this assumption based on experimental results (see Figure 2.3).

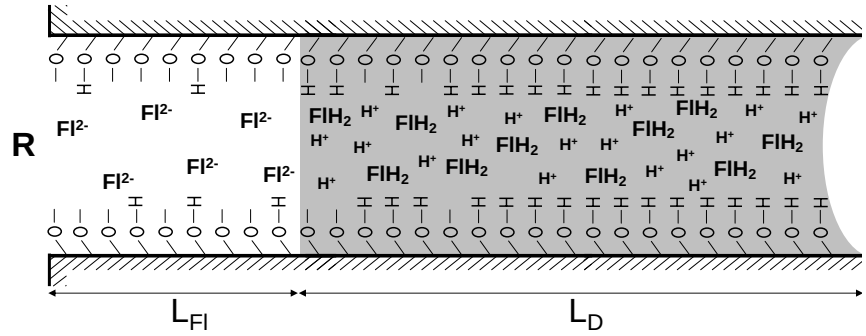

Figure 2.3 Axial cross-section of a filling nanochannel. R indicates the reservoir from which the nanochannel is filled. L_{Fl} and L_D correspond to the fluorescent and dark zone of the channel, respectively. In the fluorescent zone the pH is that of the introduced solution where fluorescein is present mainly as doubly charged anions (Fl^{2-}). The fluid in the dark zone contains an excess of protons, with $pH = pH_{pzc}$ and fluorescein is mainly present as the uncharged fluorescein molecule (FlH_2), having negligible fluorescence.

We denote the length of the fluorescent and dark zone as L_{Fl} and L_D respectively as shown in Figure 2.3. The protons released from the walls in the fluorescent zone of the channel are responsible for protonating the fluorescein in the dark zone, so that L_{Fl} can be used to deduce the released number of protons, $N_{H^+_{released}}$ via

$$N_{H^+_{released}} = N_S \Theta^- L_{Fl} 2(h+w) \tag{2.3}$$

where Θ^- is the fraction of the surface groups that is negatively charged, N_S the total number of SiOH sites, taken to be $4.6 \cdot 10^{18}$ groups per m^2 [97], h (m) is the measured height and w (m) the width of the channel; see also Table 2.2 for a description of the general variables in the equations.

The amount of protons absorbed by the solution in the dark zone (L_D), $N_{H^+_{absorbed}}$, can then be expressed using the number of protons necessary to change the pH from its initial value to the point of zero charge, B_S (in mol/m^3), as

$$N_{H^+_{absorbed}} = N_A B_S L_D h w \tag{2.4}$$

with N_A Avogadro's constant. B_S includes the concentration of protons needed to protonate fluorescein and the concentration required to establish a pH equal to pH_{pzc}. If a buffer is present, the concentration of protons needed to protonate the buffer is calculated based on the composition according to Table 2.1, e.g., 0.2 mol/L Tris buffer brought to pH 8.4 with 0.072 mol/L HCl requires 0.128 mol/L of protons.

Typical results for the position of the fluid front and fluorescent front are given in Figure 2.4. The linear relationship between the position of the fluid front and the square root of time is in good agreement with the Washburn equation (2.2)

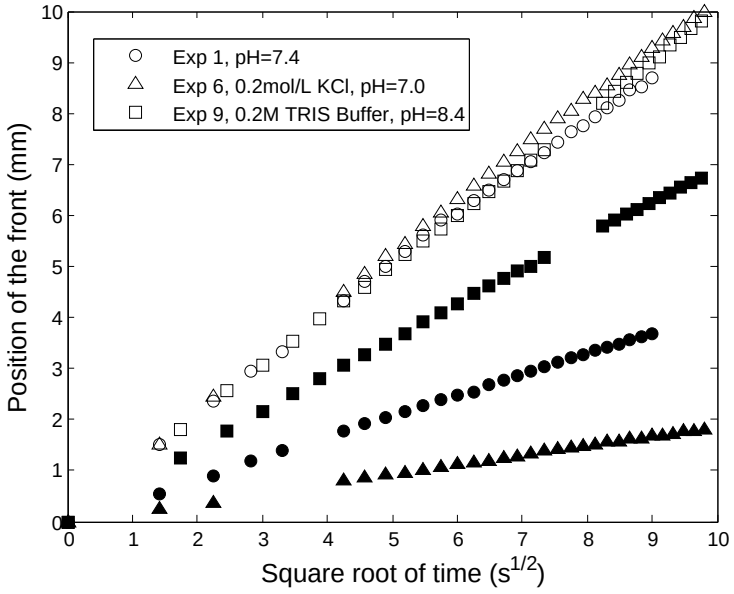

Figure 2.4 Position of the meniscus (empty symbols) and the fluorescent front (filled symbols) versus the square root of time for experiments 1, 6 and 9. All graphs could be linearly fitted using a least squares method with a value of $R^2 > 0.99$.

and earlier results reported by Tas et al[95]. A constant ratio between the positions of the meniscus and the fluorescent front is observed, with the fluorescing zone of the channel linearly dependent on the amount of channel filled. This means that the ratio L_D/L_{Fl} is constant per experiment and can be used to characterize it. For example, the experiments 1, 6, and 9, (shown in Figure 2.4) have a ratio of 0.41, 0.18, and 0.70, respectively. This actually supports our assumption that axial proton diffusion does not have a significant effect on our experiments. If this would be the case, this would show up as a nonlinearity of the plot of the fluorescent front against time toward the end of the experiment, which is not seen in the data.

We can derive the number of protons released per area of wall, $N_{H^+_{exp}}$, as a function of the observed ratio of dark and fluorescent zones, by equating the absolute amounts of released and absorbed protons (eqs 2.3 and 2.4) and using $h << w$:

$$N_{H^+_{exp}} \equiv N_S\Theta^- = N_A B_S h \frac{1}{2}\frac{L_D}{L_{Fl}} \tag{2.5}$$

Equation 2.5 provides an experimental expression for the amount of released protons.

2.3.3 Theoretical amount of protons released.

We will now construct a theoretical model to describe the theoretical amount of released protons which can be verified by comparing it to the experimental data. When the channel is filled with an aqueous solution it interacts with the silanol groups as described by the following surface reactions

$$SiOH_2^+ \rightleftharpoons SiOH + H_S^+ \tag{2.6}$$

characterized by the dissociation constant K_{a1} and

$$SiOH \rightleftharpoons SiO^- + H_S^+ \tag{2.7}$$

characterized by the dissociation constant K_{a2} and with H_S^+ the concentration of protons at the surface. pK_{a2} has been reported to be 6.7[98] and pK_{a1} has been reported to be -1.9[99].

When protons are released into solution, this induces a negative potential on the silicon oxide surface, Ψ_0, and a surface charge σ_0. The surface charge depends on the amount of SiOH sites, N_S, the dissociation constants K_{a1} and K_{a2} and the proton activity at the surface $a_{H_S^+}$ and is given by[91]:

$$\sigma_0 = qN_S \left(\frac{a_{H_S^+}^2 - K_{a1}K_{a2}}{a_{H_S^+}^2 + K_{a1}a_{H_S^+} + K_{a1}K_{a2}} \right) \tag{2.8}$$

The negative potential affects the distribution of ions in the solution directly near this surface such that there is a region containing its counter charge. This system of charged wall and the region containing the counter charge density of ions in solution is known as the electrical double layer (Figure 2.5).

At some distance from the surface, at least several Debye lengths, the bulk solution is characterized by its bulk number concentration of ions, n^0 (m^{-3}, for a 1:1 ion equal to the ionic strength) and bulk pH, pH_B. The difference in proton activity between surface and electroneutral bulk is according to Boltzmann

$$pH_S = pH_B + \Psi_0 \frac{q}{2.3kT} \tag{2.9}$$

with k Boltzmann's constant, q the elementary charge, and T temperature. This equation can be used to express measured bulk pH into σ_0 via eq 2.8 and demonstrates the dependence of σ_0 on pH_B. The combination of Poisson's equation with Boltzmann's equation also gives an expression for the surface charge[48]:

$$\sigma_0 = \sqrt{8kT\varepsilon\varepsilon_0 n^0} \sinh\left(\frac{q\Psi_0}{2kT}\right) \tag{2.10}$$

This equation demonstrates the dependence of σ_0 on the ionic strength n^0 and it can be used to calculate Ψ_0. The charge on the electrolyte side of the double

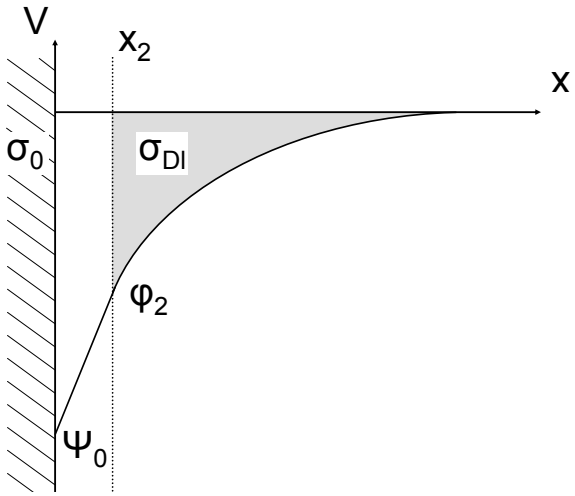

Figure 2.5 Schematic representation of potential V versus the distance x from the silicon oxide wall. Ψ_0 is the potential at the wall. x_2 is the position of the Stern plane, the plane of closest approach of ions toward the surface, having the potential ϕ_2. The region from the wall to the Stern plane is called the Stern layer. σ_0 (eq. 2.8 and eq. 2.13) indicates the surface charge per m^2 from deprotonated silanol groups at x=0. σ_{Dl} is the countercharge to σ_0 per m^2 (eq. 2.11), composed of ions located in the area beyond the Stern plane, the so-called diffuse part of the double layer (gray region).

layer, σ_{DL} is equal and of opposite sign to the surface charge σ_0 and can be described as a function of a double layer capacitance C_{DL} (in F/m^2) and the surface potential Ψ_0:

$$\sigma_{DL} = -C_{DL}\Psi_0 = -\sigma_0 \tag{2.11}$$

For our model we make use of the refinement of double layer theory as proposed by Stern[48]. Ions have a finite size and the closest distance they can approach the surface, equal to the radius of an ion, is the so-called Stern plane. This causes the potential drop across the double layer to have a discontinuity (Figure 2.5). Directly near the surface the double layer is described by the potential drop across the Stern plane from Ψ_0 to ϕ_2. The capacitance of the Stern layer, C_{Stern} (in F/m^2) is therefore given by:

$$C_{Stern} = \frac{\sigma_0}{\Psi_0 - \phi_2} \tag{2.12}$$

Beyond the Stern plane the surface charge density in the diffuse layer of counter ions is now described by:

$$\sigma_0 = \sqrt{8kT\varepsilon\varepsilon_0 n^0}\sinh\left(\frac{q\phi_2}{2kT}\right) \tag{2.13}$$

and the capacitance of the diffuse part of the double layer, C_{Diff} is given by:

$$C_{Diff} = \frac{\sigma_0}{\phi_2} \tag{2.14}$$

The double layer capacitance is given by the Stern and diffuse layer capacitances placed in series[48]:

$$C_{DL} = \frac{1}{C_{Stern}^{-1} + C_{Diff}^{-1}} \tag{2.15}$$

To describe titration experiments of SiO_2 surfaces, colloid experiments typically take values for C_{Stern} of 0.8 to 1.4 F/m^2 [100]. It has also been argued that for a porous well ordered planar surface values for C_{Stern} between 0.8 to 1.7 F/m^2 should be assumed[100]. As these values for C_{Stern} vary considerably and strongly affect our model, we used C_{Stern} to fit the measurement results (2.5), with the constraint of one C_{Stern} for all experiments.

From the above eqs 2.8 to 2.15 we can derive σ_0 via an iteration procedure (see footnote [b]), and therefore the amount of protons released per surface area into the bulk solution:

$$N_{H^+_{theory}} = \frac{\sigma_0}{q} \tag{2.16}$$

which can be fitted to $N_{H^+_{exp}}$ (eq 2.5). An overview of constants and parameters used for fitting is given in Table 2.2.

2.4 Results & Discussion

2.4.1 Theoretical results.

Our theoretical model shows how the capacity of the solution to take up protons, via a buffer and via fluorescein itself, affects the position of the fluorescent front. More buffer for this reason leads to a larger fluorescent zone. The model shows how a higher pH of the introduced solution increases the amount of protons per nm^2 to be released (eq 2.9, a higher pH induces a more negative surface potential effectuated by proton release). It also shows how the ionic strength affects proton release (eq 2.13, for a more in depth explanation see footnote [c]) as is seen in

[b] The iteration procedure, has the ionic strength and measured pH (Table 2.1), as well as the surface properties stated above (Table 2.2), as input parameters. Choosing a starting value for Ψ_0, it is entered into Boltzmann's equation (eq 2.9) giving the surface activity of protons, which is used to calculate σ_0 (eq 2.8) and subsequently applied to yield ϕ_2 (eq 2.13). Finally a new value for Ψ_0 is calculated from $\Psi_0 = \phi_2 + \sigma_0 / C_{Stern}$ (eq 2.12) and reentered into the Boltzmann equation(eq 2.9). The stable value for σ_0 is then used for equation 2.16.

[c] The effect of the ionic strength is demonstrated by the Debye-Hückel approximation[48] of C_{Diff} as $C_{Diff} = \varepsilon / \lambda_D$, with λ_D the Debye length. A higher ionic strength, n_0, decreases the Debye length and increases C_{Diff}, leading to a larger negative surface charge density and a larger proton release to titrate the solution.

Table 2.2 Constants and parameters used in fitting the data.

Constants	description	value
q	elementary charge	1.6022x10^{-19} C
k	Boltzmann's constant	1.38x10^{-23} J/K
ε_0	permittivity of free space	8.8542x10^{-12} C^2/Nm^2
N_A	Avogadro's constant	6.022x10^{23} mol^{-1}
Experimental variables		Remarks
T	temperature	297 K
ε	relative permittivity of water	80, in presence of salt
N_S	silanol groups per m^2	4.6x10^{18} [97]
h	measured channel height	Table 2.1
pH_B	measured bulk pH of introduced solutions	Table 2.1
L_D	length of dark zone	Figure 2.4
L_{Fl}	length of fluorescent zone	Figure 2.4
Calculated variables		Remarks
pH_S	calculated pH at the surface	eq 2.9
pH_{pzc}	pH at point of zero charge of SiO_2	average of pK_{a1} & pK_{a2}
n^0	ionic strength in the bulk	m^{-3}, derived from Table 2.1
B_S	required protons to titrate from pH_B to pH_{pzc}, includes those for fluorescein, and any buffer.	mol/m^3 derived from Table 2.1 & pH_{pzc}
$N_{H^+_{exp}}$	amount of protons released per m^2 of wall	calculated from experiment, see eq 2.5
Ψ_0	surface potential in V, calculated with fitted variables and Table 2.1	solved numerically, see footnote [b] p37
ϕ_2	potential at the Stern plane in V calculated with fitted variables and Table 2.1	solved numerically, see footnote [b] p37
σ_0	surface charge in C/m^2, calculated with fitted variables and Table 2.1	solved numerically, see footnote [b] p37
$N_{H^+_{theory}}$	theoretical amount of released protons per m^2 of wall	derived from σ_0 eq. 2.16
Fitted variables		Remarks
pK_{a1}	dissociation constant eq. 2.6	-1.9 [99] selected for the fitting of Fig.2.7
pK_{a2}	dissociation constant eq. 2.7	fitted
C_{Stern}	Stern capacitance in F/m^2, affects H^+_{theory}, eq. 2.16	fitted

our experiments. Hereby the buffer ions are incorporated in the determination of the ionic strength. Figure 2.6 shows the theoretically calculated amount of deprotonated groups as a function of pH and ionic strength. Using this model we fitted our experimental results.

2.4.2 Fitting results.

The parameter space we investigated to fit the data was pK_{a2} = [4 to 7.5] and pK_{a1} = [-2.4 to 0]. Each pair of pK_a values was used to fit the data of the unbuffered and buffered results, under the constraint that C_{Stern} is equal for all data, using eqs 2.8 to 2.15 according to the iteration procedure described in footnote [a] p37. As

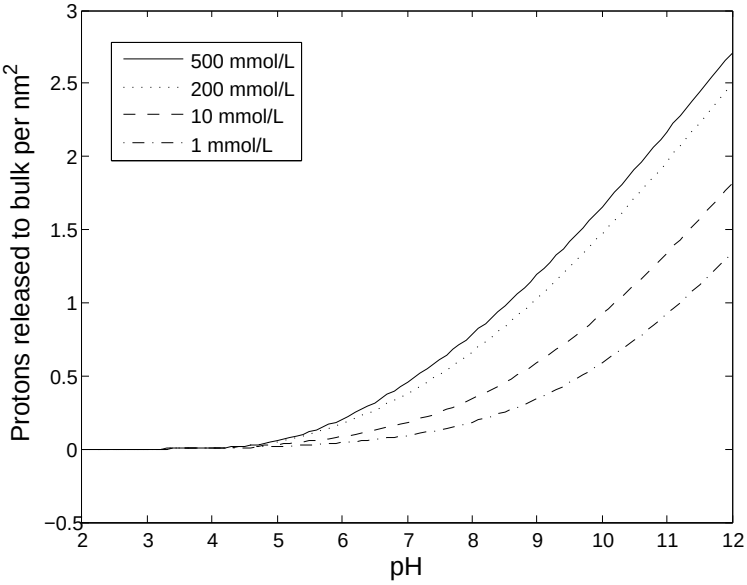

Figure 2.6 Theoretical amount of deprotonated silanol groups per nm^2 as a function of pH. The different curves, belonging to 1, 10, 200, and 500 mmol/L of KCl, show the effect of the ionic strength on proton release, with more salt inducing a higher release, which will be observed as a shorter fluorescent zone.

a side note, interestingly, it appears that the fitting results could be described by the empirical relation C_{Stern} = 2.32x10$^{-4}e^{3.77pH_{pzc}}$ (R^2 = 0.99) and therefore many pairs of dissociation constants pK_{a1} and pK_{a2} yielded a good fit as long as they gave the same pH_{pzc}.

Figure 2.7 shows measured data points as well as fitted curves, displaying the amount of released protons as a function of ionic strength. To generate Figure 2.7, we chose pK_{a1} = -1.9 based on literature[99], which yielded a dissociation constant pK_{a2} = 6.77 close to the literature value of 6.7 reported by Davis et al.[98], accepting a somewhat high C_{Stern} of 2.30 F/m^2.

High values of C_{Stern} (greater than 1.7 F/m^2) for a nonporous surface can be attributed to complexation of ions in solution with silanol groups[98]. This is because ionic complexation has been reported to shift the point of zero charge[101] from its value as the mean of the pKa's, when only protons are the potential determining ions, to another value. According to our empirical relation a slight difference in pH_{pzc} results in a significant change in C_{Stern}, e.g. compared to $pH_{pzc} = 2.44$ with $C_{Stern} = 2.3$ F/m^2, $pH_{pzc} = 2.36$ yields $C_{Stern} = 1.7$ F/m^2. A second explanation for high values of C_{Stern}, according to Hiemstra et al.[100] is the silicon oxide surface having a less condensed surface structure and the presence of reactive surface groups protruding from the surface.

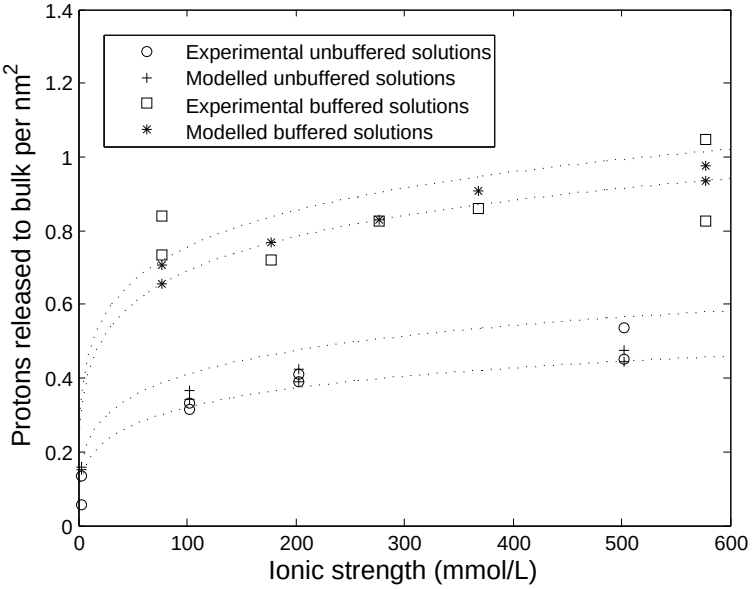

Figure 2.7 Results of the experiments, $N_{H^+_{exp}}$, fitted with the model, $N_{H^+_{theory}}$. Fits were made using the input and fitting parameters from Tables 2.1 and 2.2, with the dissociation constants pK_{a1} = 6.77 and pK_{a2} = -1.90 and therefore a pH_{pzc} = 2.44. A value of C_{Stern} = 2.30 F/m^2 led to the optimal fit with R^2 = 0.93 for the unbuffered solutions and R^2 = 0.37 for buffered solutions. The data point for the buffered solution at an ionic strength of 386 mmol/L has a buffer strength of 1 mol/L, the others 0.2 mol/L. The dashed lines indicate the modeled values corresponding to the extremes of pH in the introduced solutions, from top to bottom, pH = 8.6, pH = 8.4, pH = 7.4, and pH = 7.0.

A good fit was achieved for the solutions containing fluorescein and KCl, R^2=0.93, and a lesser fit was found for the solutions containing TRIS buffer R^2=0.37, due to the spread in experimental results (See variation in duplicate experiments in Figure 2.7).

Figure 2.7 shows that the variation in amount of released protons is reasonably explained by the variation in ionic strength and the pH of the filling fluid. On the other hand the buffer concentration in the filling fluid does not affect the released amount of protons per wall area (apart from its contribution to the ionic strength). This is indeed expected since the model gives an amount of protons released per wall area based only on the equilibrium with an infinite solution of the initial pH and ionic strength. Though the buffer concentration affects the ratio between the dark and fluorescent zone, this is incorporated in eq 2.5, leading to an amount of protons released per wall area independent from buffer concentration.

2.4.3 Buffer effects.

Figure 2.7 shows a large spread in the duplicate measurements of several buffered solutions. This is probably caused by substantial variations in the buffer composition. Inspection of Table 2.1 shows that the measured pH of the Tris-buffered solutions varied between 8.4 and 8.6, though all solutions were prepared by adding 0.072 mol/L HCl to a 0.2 mol/L Tris solution. These pH differences would indicate substantial differences in buffer capacity of the resulting solutions, affecting the value of B_S and $N_{H^+_{exp}}$ (eq 2.5).

2.4.4 Fluorescence front.

The results show a release of approximately 0.8 protons per nm^2 for the solutions around pH = 8.5, and 0.4 protons per nm^2 for the unbuffered solutions, pH = 7-7.4. We would like to stress the effect that such an amount of released protons has in shallow channels of 50 nm in height and arbitrary width. For a released amount of 0.5 protons/nm^2, 1 proton is released into the 50 nm^3 between the two walls or 0.02 protons per nm^3 (corresponding to a concentration of 33 mmol/L). To titrate a solution of 0.6 molecules per nm^3 (1 mol/L) the solution therefore has to pass only 30 nm of channel.

Together with the very fast equilibration in radial direction, this can explain our observation of a sharp fluorescence boundary for example in Figure 2.1. The argumentation for this is as follows: the protons diffusing axially into the fluorescent zone will be buffered by the solution, whereas fluorescein and/or buffer molecules that diffuse into the dark zone will be instantly protonated. Even if axial diffusion contributes significantly to proton transport relative to the flow of solution, this transient zone between dark and fluorescent regions will be the first to be in contact with undeprotonated wall and become protonated to pH_{pzc}. This effectively conserves the sharpness of the boundary between the dark and fluorescent zones, as is observed in our experiments.

2.5 Conclusion

A new phenomenon was observed unique to nanofluidics, namely a decrease in the fluorescent activity of fluorescein during capillary filling. The observed dark and fluorescent regions can be explained by acidification of the solution via deprotonation of the silanol groups at the wall. This mechanism could be verified by establishing a model based on the double layer theory and fitting this to the data. This mechanism represents a unique way to titrate a solution without adding additional counterions and to study the properties of a surface.

As chemical analysis in nanochannels is a growing field of research, the understanding of the effects of the nanostructure walls, due to a high surface to volume ratio, on the solution pH and the resulting changes in wall potential are of

great significance. Importantly, this will occur in all transient cases, which means not only during filling but also when the solution pH or ionic strength is changed. This will be especially important for the analysis of biological samples because of its complex matrix composition. Fortunately, these effects can be modeled as demonstrated in this study.

2.6 Acknowledgements

Support from Nanoned (flagship Nanofluidics) is gratefully acknowledged. We also acknowledge Dr. Heiko van der Linden for useful comments on the manuscript.